Step-wise modifications of the Vegetation Optimality Model

Remko C. Nijzink[1], Jason Beringer[2], Lindsay B. Hutley[3], and Stanislaus J. Schymanski[1]

[1]Luxembourg Institute of Science and Technology, Environmental Research and Innovation, Catchment and Eco-hydrology Research Group, Belvaux, Luxembourg
[2]School of Agriculture and Environment, The University of Western Australia, Crawley, WA, Australia, 6909
[3]Research Institute for the Environment and Livelihoods, Charles Darwin University, Darwin, NT, Australia, 0909

Correspondence: R.C. Nijzink (remko.nijzink@list.lu)

Abstract.

The Vegetation Optimality Model (VOM, Schymanski et al., 2009, 2015) is an optimality-based, coupled water-vegetation model that predicts vegetation properties and behaviour based on optimality theory, rather than calibrating vegetation properties or prescribing them based on observations, as most conventional models do. In order to determine whether optimality theory
5   can alleviate common shortcomings of conventional models, as identified in a previous model inter-comparison study along the North Australian Tropical Transect (NATT) (Whitley et al., 2016), a range of updates to previous applications of the VOM have been made for increased generality and improved comparability with conventional models. To assess in how far the updates to the model and input data would have affected the original results, we implemented them one-by-one while reproducing the analysis of Schymanski et al. (2015).

10   The model updates included extended input data, the use of variable atmospheric CO_2-levels, modified soil properties, implementation of free drainage conditions, and the addition of grass rooting depths to the optimized vegetation properties. A systematic assessment of these changes was carried out by adding each individual modification to the original version of the VOM at the flux tower site of Howard Springs, Australia.

The analysis revealed that the implemented changes affected the simulation of mean annual evapo-transpiration (ET) and
15   gross primary productivity (GPP) by no more than 20%, with the largest effects caused by the newly imposed free drainage conditions and modified soil texture. Free drainage conditions led to an underestimation of ET and GPP, whereas more fine-grained soil textures increased the water storage in the soil and resulted in increased GPP. Although part of the effect of free drainage was compensated for by the updated soil texture, when combining all changes, the resulting effect on the simulated fluxes was still dominated by the effect of implementing free drainage conditions. Eventually, the relative error for the mean
20   annual ET, in comparison with flux tower observations, changed from an 8.4% overestimation to an 10.2% underestimation, whereas the relative errors for the mean annual GPP stayed similar with a change from 17.8% to 14.7%. The sensitivity to free drainage conditions suggests that a realistic representation of groundwater dynamics is very important for predicting ET and GPP at a tropical open-forest savanna site as investigated here. The modest changes in model outputs highlighted the robustness of the optimization approach that is central to the VOM architecture.

1 Introduction

Novel modelling approaches that are able to explicitly model vegetation dynamics, may lead to an overall improved understanding of flux exchanges with the atmosphere. Recent model inter-comparison studies also reveal that novel model approaches are needed, especially related to vegetation dynamics (e.g. Whitley et al., 2016). Therefore, we use here optimality theory to predict the variation and dynamics of vegetation cover, root systems, water use and carbon uptake without the need for site-specific input about vegetation properties. The theory is based on the premise that the net carbon profit (NCP), which is the difference between carbon assimilated by photosynthesis and carbon expended on construction and maintenance of all the plant tissues needed for photosynthesis and water uptake and storage, is an appropriate measure of plant fitness, given that assimilated carbon is a fundamental resource of plant growth, development, survival and reproduction. The theory further assumes that construction and maintenance costs of plant organ functionality are general and therefore transferable between species and sites. Hence, the costs and benefits at different sites are determined in a consistent way, leading to vegetation properties that solely depend on physical conditions, such as meteorological forcing, soils and hydrology. As a result, this leads to a systematic and consistent explanation of vegetation behaviour under different external conditions at different sites.

These optimality principles were employed in the Vegetation Optimality Model (VOM, Schymanski et al., 2009, 2015). The VOM is a coupled water-vegetation model that optimizes vegetation properties to maximize the Net Carbon Profit (NCP) in the long-term (20-30 years) for given climate and physical properties at the site under consideration. The NCP is defined as the difference between the total carbon amount assimilated by photosynthesis, and the total carbon costs for the maintenance of leaf area, photosynthetic capacity and root surface area, as described in Schymanski et al. (2007, 2008b). The VOM has been previously applied by Schymanski et al. (2009) and Schymanski et al. (2015) at Howard Springs, a flux tower site in the North Australian Tropical Transect (NATT, Hutley et al., 2011). The NATT consists of multiple flux tower sites along a precipitation gradient from north to south, which allows for a more systematic testing of the VOM under different climatological circumstances. The NATT has been used previously in an intercomparison of terrestrial biosphere models (TBMs) by Whitley et al. (2016), which revealed that lacking or wrong vegetation dynamics and incorrect assumptions about rooting depths have a strong influence on the performance of state-of-the-art TBMs. In contrast to these TBMs, the VOM predicts rooting depths and vegetation dynamics, and provides therefore a novel approach for the simulation of these savanna sites.

To assess in how far the optimality-based simulation of rooting depths, tree cover and vegetation dynamics may alleviate the shortcomings of TBMs identified by Whitley et al. (2016), we propose to run the VOM using the same input data and similar physical boundary conditions at the different sites as in Whitley et al. (2016). In the simulations by Whitley et al. (2016), all TBMs were run under the assumption of a freely draining soil column, even though studies suggest an influence of groundwater on the resulting fluxes (York et al., 2002; Bierkens and van den Hurk, 2007; Maxwell et al., 2007). Free draining conditions can be mimicked in the VOM by setting drainage parameters to very fast drainage and the critical water table for the onset of drainage very low (see below).

In previous applications of the VOM (Schymanski et al., 2009, 2015), atmospheric CO_2 concentrations were assumed constant over the entire modelling period, whereas for inter-comparison with other models, we should use measured CO_2-

levels, which have increased considerably over the past years (Keeling et al., 2005). Previous applications of the VOM also
60   prescribed a grass rooting depth of 1 m, arguing that due to the presence of a hard pan at Howard Springs, only tree roots could
penetrate into deeper layers. Since we do not know if such features exist at the other sites along the NATT, rooting depth of
seasonal vegetation should be optimised in a similar way as that of perennial vegetation.

   To assess to what extent the various changes influence the VOM-results, a new set-up of the VOM was applied to the same
flux tower site in Australia, Howard Springs, as in Schymanski et al. (2009, 2015). This technical note describes the changes
65   to the VOM since its last application by Schymanski et al. (2015), and how they affect the results of the VOM one-by-one and
in combination.

2   Methodology

All steps in the process, from pre- and post-processing to model runs, were done in an open science approach using the
RENKU[1] platform. The workflows including code and input data can be found online[2]. In the following, we briefly describe
70   the study site, the VOM, and the various modifications done in this study, compared to Schymanski et al. (2015).

2.1   Study site

The study site is Howard Springs (How-AU), which was previously used by Schymanski et al. (2009) and Schymanski et al.
(2015) and provides a long record of carbon dioxide and water fluxes starting from 2001 (Beringer et al., 2016). Howard Springs
is the wettest site (average precipitation of 1747 mm/year (SILO Data Drill, Jeffrey et al., 2001, calculated for 1980-2017))
75   along the North Australian Tropical Transect (NATT, Hutley et al., 2011), which has a strong precipitation gradient from north
to south, with a mean annual precipitation around 500 mm/year at the driest site. The vegetation at Howard Springs consists
of a mostly evergreen overstorey (mainly *Eucalyptus miniata* and *Eucalyptus tetrodonta*) and an understorey dominated by
annual *Sorghum* and *Heteropogon* grasses. The soils at Howard Springs are well-drained red and grey kandosols, and have a
high gravel content and a sandy loam structure.

2.2   Vegetation Optimality Model

The Vegetation Optimality Model (VOM, Schymanski et al., 2009, 2015) is a coupled water and vegetation model, that opti-
mizes vegetation properties by maximizing the Net Carbon Profit. The model code and documentation can be found online[34]
and version v0.5[5] of the model was used here. A general description is given below, whereas a more detailed description can
be found at Schymanski et al. (2009, 2015).

---

[1]https://renkulab.io/
[2]https://renkulab.io/gitlab/remko.nijzink/vomcases
[3]https://github.com/schymans/VOM
[4]https://vom.readthedocs.io
[5]https://doi.org/10.5281/zenodo.3630081
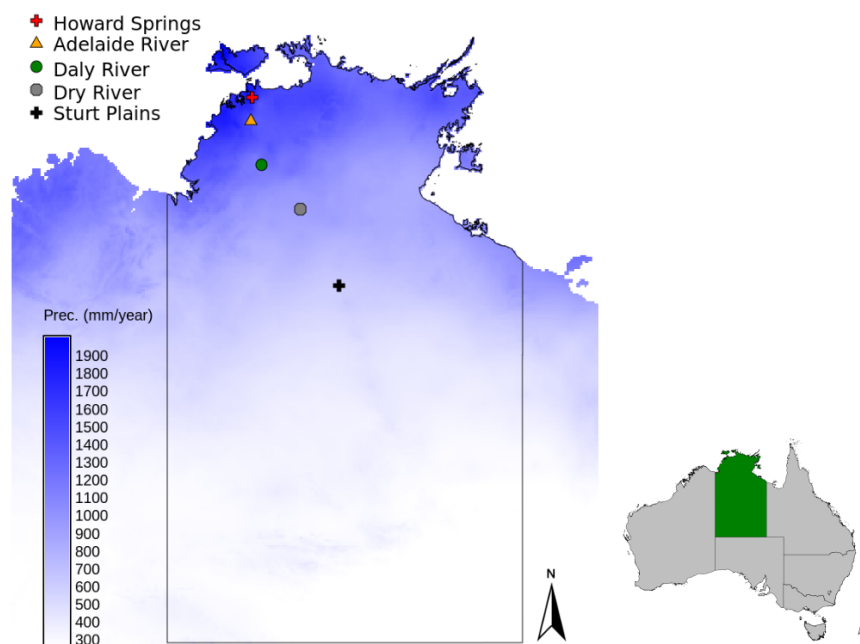
Figure 1. Location of the Howard Springs site, together with the other flux tower sites that are part of the North Australian Tropical Transect in the Nortern Territory of Australia, with the mean annual precipitation shown in the blue colorscale (SILO Data Drill, Jeffrey et al., 2001, calculated for 1980-2017).

2.2.1   Vegetation model

The VOM schematizes the ecosystem as two big leaves, one representing the seasonal vegetation (grasses) and one representing the perennial vegetation (trees). Photosynthesis was modelled according to Schymanski et al. (2007), who simplified the canopy-gas exchange model of von Caemmerer (2000) for C_3-plants. The model computes CO_2-uptake as a function of irradiance, atmospheric CO_2-concentrations, temperature, photosynthetic capacity, projected foliage cover and stomatal conductance, whereby photosynthetic capacity, projected foliage cover and stomatal conductance are optimized dynamically in a way to maximize the overall Net Carbon Profit (NCP) of the vegetation over the entire simulation period. Optimization is possible due to the carbon costs associated with each of these variables: photosynthetic capacity is linked to maintenance respiration, projected cover to the turnover and maintenance of leaf area, while stomatal conductance is linked to transpiration (depending on the atmospheric vapour pressure deficit) and hence root water uptake costs and limitations. Root water uptake is modelled following an electrical circuit analogy, where the water potential difference between the plant and each soil layer drives the flow. Here, the root surface area and soil hydraulic conductivity in each soil layer determine the resistance (Schymanski et al., 2008b). The root surface area, in return, generates carbon costs for maintenance and the vertical distribution in the soil profile is optimized in a way to satisfy the canopy water demand with the minimum possible total root surface area.

Table 1. Characteristics of the Howard Springs site. Vegetation data from Hutley et al. (2011), Hutley (2015) and Whitley et al. (2016), with Eucalyptus (Eu.), Erythrophleum (Er.), Hetropogan (He.). Meteorological data is taken from the SILO Data Drill (Jeffrey et al., 2001) for the model periods of 1-1-1980 until 31-12-2017, with the potential evaporation calculated according to the FAO Penman-Monteith formula (Allen et al., 1998). The ratio of the net radiation Rn with the latent heat of vaporization λ mutiplied with the precipitation P, is defined here as the aridity $Rn/\lambda P$. Tree cover is determined as the minimum value of the mean monthly projective cover based on fPAR-observations (Donohue et al., 2013). The maximum grass cover was found by subtracting the tree cover from the remotely sensed projective cover.

Study Site	Howard Springs
FLUXNET ID	AU-How
Coordinates	12.49S
	131.35E
Prec. (mm year^{-1})	1747
Pot. evap. (mm year^{-1})	1763
Aridity. (-)	1.03
Net Rad. (MJ m^{-2} year^{-1-1})	4392
Mean max. temp. [^{o}C]	37.5
Mean min. temp. [^{o}C]	27.4
Tree cover (%)	39.8
Max. grass cover (%)	44.3

Species	
Overstorey	*Eu. miniata*
	Eu. tetrodonta
	Er. chlorostachys
Understorey	*Sorghum spp.*
	He. triticeus

2.2.2 Long-term optimization

100 The rooting depths of the perennial trees and the seasonal grasses ($y_{r,p}$ and $y_{r,s}$) as well as the foliage projected cover of the perennial vegetation ($M_{A,p}$) are derived by optimizing these properties for the long-term, assuming that these do not vary significantly during the simulation period (20-30 years). Similarly, water use strategies of both the perennial and the seasonal vegetation component are assumed to be a result of long-term natural selection for a given site, and are also optimized in order to maximize the Net Carbon Profit. To do so, the water use strategy was expressed as a functional relation between

105 the marginal water cost of assimilation (Cowan and Farquhar, 1977), represented by λ_p and λ_s for perennial and seasonal
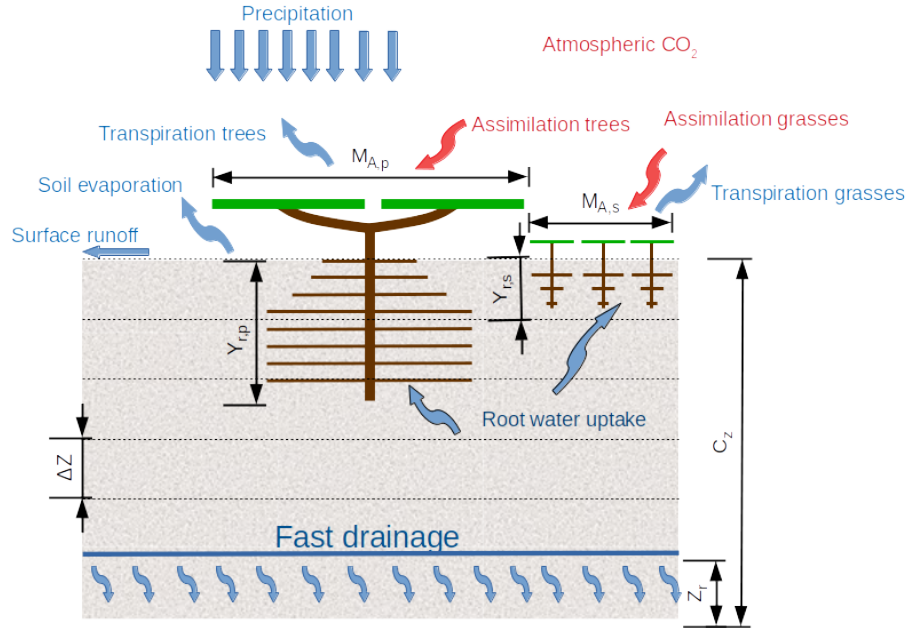
Figure 2. Schematization of the Vegetation Optimality Model as two big leaves, with $M_{A,p}$ and $M_{A,s}$ the fractional cover of perennial trees and seasonal grasses respectively, $y_{r,p}$ and $y_{r,s}$ the rooting depths of the perennial trees and seasonal grasses respectively, ΔZ the soil layer thickness, C_Z the total soil depth, and Z_r the drainage depth.

vegetation respectively, and the sum of water suction heads (h_i) in all soil layers within the root zone, after Schymanski et al. (2009):

$$\lambda_s = c_{\lambda f,s} \left(\sum_{i=1}^{i_{r,s}} h_i \right)^{c_{\lambda e,s}} \tag{1}$$

$$\lambda_p = c_{\lambda f,p} \left(\sum_{i=1}^{i_{r,p}} h_i \right)^{c_{\lambda e,p}} \tag{2}$$

110 where $c_{\lambda f,s}$, $c_{\lambda e,s}$, $c_{\lambda f,p}$ and $c_{\lambda e,p}$ are the optimized parameters, while $i_{r,p}$ and $i_{r,s}$ represent the number of soil layers reached by perennial and seasonal roots, respectively. After the establishment of the optimized water use parameters in Eqs. 1 and 2 (i.e. the long-term relation between soil water marginal water costs), the values of λ_p and λ_s are calculated for each day separately and then used to simulate the diurnal variation in stomatal conductance using Cowan-Farquhar optimality (Cowan and Farquhar, 1977; Schymanski et al., 2008a). The values of $c_{\lambda f,s}$, $c_{\lambda e,s}$, $c_{\lambda f,p}$ and $c_{\lambda e,p}$ essentially express how quickly

115 plants reduce water use as soil water suction increases during dry periods. The slower λ_s and λ_p are reduced in response to drying soil, the larger the root costs are as the root systems are adjusted to satisfy the canopy water demand. The parameters

$(c_{\lambda f,s}, c_{\lambda e,s}, c_{\lambda f,p}$ and $c_{\lambda e,p})$ are optimized and constant in the long-term, along with y_r and $M_{A,p}$, to maximize the total NCP over the entire simulation period.

2.2.3 Short-term optimization

120 Some vegetation properties, such as seasonal vegetation cover ($M_{A,s}$), photosynthetic capacities and root surface area distributions of the seasonal and perennial vegetation component, are allowed to vary on a daily basis to reflect their dynamic nature. Their values are hence optimized from day to day in a way to maximize the daily NCP. This is done by using three different values for each of these vegetation properties, the actual value and a specific increment above and below this value every day, and at the end of the day the combination of values that would have achieved the maximum NCP on the present day is selected

125 for the next day. See Schymanski et al. (2009, 2015) for details.

2.2.4 Carbon cost functions

As mentioned above, different carbon cost functions are used to quantify the maintenance costs for different plant organs. The carbon cost related to foliage maintenance is based on a linear relation between the total leaf area and a constant leaf turnover cost factor:

130 $$R_f = L_{AIc} c_{tc} M_{A,p} \tag{3}$$

where L_{AIc} is the clumped leaf area (set to 2.5 (Schymanski et al., 2007)), c_{tc} is the leaf turnover cost factor (set to 0.22 μmol^{-1} s^{-1} m^{-2}, (Schymanski et al., 2007)) and $M_{A,p}$ is the perennial vegetation cover fraction.

The costs for root maintenance were defined as (Schymanski et al., 2008b):

$$R_r = c_{Rr} \left(\frac{r_r}{2} S_{A,r} \right) \tag{4}$$

135 where c_{Rr} is the respiration rate per fine root volume (0.0017 mol s^{-1} m^{-3}), r_r the root radius (set to 0.3*10^{-3} m) and $S_{A,r}$ the root surface area per unit ground area (m^{2}m^{-2}). The values used in this parameterization stem from observations on citrus plants, as described by Schymanski et al. (2008b).

Water transport costs are assumed to depend on the size of the transport system, from fine roots to the leaves. The canopy height is not modelled in the VOM, and the transport costs are therefore just a function of rooting depth and vegetated cover:

140 $$R_v = c_{rv} M_A y_r \tag{5}$$

where c_{rv} is the cost factor for water transport (mol m^{-3} s^{-1}), M_A the fraction of vegetation cover ($-$), and y_r the rooting depth (m). The costfactor c_{rv} was set to 1.0 μmol m^{-3} s^{-1} by Schymanski et al. (2015) after a sensitivity analysis for Howard Springs, which is also adopted here.

2.2.5 Water balance model

145 As described in Schymanski et al. (2015), the soil is schematized as a permeable block containing an unsaturated zone and a saturated zone, overlaying an impermeable bedrock with a prescribed drainage level. The model simulates a variable water table based on the vertical fluxes between horizontal soil layers and a drainage flux computed as a function of the water table elevation. Here, the thickness of soil layers was prescribed to 0.2 m, based on a sensitivity analysis for Howard Springs, see also Supplement S2.

150 The hydrological parameters that determine the drainage outflow and groundwater tables are a hydrological length scale for seepage outflow, channel slope and drainage level z_r, as defined by Schymanski et al. (2015) and based on Reggiani et al. (2000). The seepage outflow is determined by the elevation difference between groundwater table and drainage level, divided by a resistance term that uses the hydrological length scale and channel slope (Eq. 10, Schymanski et al., 2008b). Originally, the hydrological length scale and channel slope were adopted from Reggiani et al. (2000) and set to 10 m and 0.033 rad,

155 respectively, in absence of more detailed knowledge about these parameters. At the same time, Schymanski et al. (2015) set the drainage level z_r and total soil thickness c_z to 10 m and 15 m, respectively, based on the local topography around the flux tower site (Schymanski et al., 2008b). This hydrological schematization resulted in groundwater tables around 5 m below the surface.

Here, the hydrological parameters were set in a way to resemble freely draining conditions, i.e. avoiding a significant in-
160 fluence of groundwater in Figure 2, for consistency with other model applications (e.g. Whitley et al., 2016), with a total soil thickness c_z of 30 m, a fast drainage parameterization with a drainage level z_r of 5 m, a length scale for seepage outflow set to 2 m and a channel slope set to 0.02 rad. As illustrated in Figure 2, when precipitation falls on this soil block, it either causes immediate surface runoff or infiltrates. Once infiltrated, it can be taken up by roots and transpired, or it can evaporate at the soil surface, or move downwards until it drains away at a depth of 30 m, well below the rooting zone (i.e. parameterized to
165 represent freely draining conditions for comparison with other models). The simulation of soil evaporation and vertical fluxes in the unsaturated zone are described in Schymanski et al. (2008b, 2015).

2.2.6 Model optimization

The VOM uses the Shuffled Complex Evolution algorithm (SCE, Duan et al., 1994) to optimize the vegetation properties listed in Table 3 for maximum Net Carbon Profit (NCP) over the entire simulation period (37 years for the new VOM set-up, from
170 1-1-1980 until 31-12-2017). The SCE-algorithm uses first an initial random seed, subdivides the parameter sets into complexes and performs a combination of local optimization within each complex and mixing between complexes to converge to a global optimum. Here, we set the initial number of complexes to 10.

2.2.7 Model input and data

A relatively long timeseries of meteorological inputs is required to run and optimize the VOM. For this reason, Schymanski
175 et al. (2015) used data from the Australian SILO Data Drill (Jeffrey et al., 2001), from which a newer version was applied to

the new VOM set-up. The meteorological data includes time series of daily maximum and minimum temperatures, shortwave radiation, precipitation, vapour pressure and atmospheric pressure. Atmospheric CO_2-levels were originally assumed constant by Schymanski et al. (2015), but in the new set-up, these were taken from the Mauna Loa CO_2-records (Keeling et al., 2005). Observed atmospheric CO_2-levels at the flux tower were not used due to the required length of the timeseries for the VOM (20-30 years). The measured meteorological variables at the flux tower sites were only used to verify the SILO meteorological data, which revealed only minor differences in the resulting fluxes of the VOM when the SILO-data was replaced for the days that flux tower observations were available (max. 6%, see Figure S4.3 in Supplement S4). See also Supplement S3, Figure S3.1 for the time series of meteorological data.

The soils, originally assumed vertically homogeneous by Schymanski et al. (2015), were parameterized based on field measurements of sand, clay and silt content provided by L. B. Hutley and J. Beringer in the top 10 cm, and the Soil and Landscape Grid of Australia (Viscarra Rossel et al., 2014a,b,c) for the deeper layers. The soils were classified into one of the soil textural groups of Carsel and Parrish (1988) based on the fractions of sand, silt and clay. Eventually, the parameters for the soil water retention model of Van Genuchten (1980) and the hydraulic conductivity were taken from the accompanying tables[6] from Carsel and Parrish (1988). See also Table 2 for the soil parameterization.

At Howard Springs, a flux tower that is part of the regional FLUXNET network OzFlux (Beringer et al., 2016), provides time series of net ecosystem exchange (NEE) of carbon dioxide and latent heat flux (LE) for model evaluation. The Dingo-algorithm (Beringer et al., 2017) was applied to the data for a gap-filled estimation of gross primary productivity (GPP) and latent heat flux (LE). LE was converted to evapo-transpiration (ET), defined here as the sum of all evaporation and transpiration processes, even though these processes are different in nature (Savenije, 2004). Eventually, the gap-filled observations of GPP and ET were compared with the modelled fluxes. The original model application of Schymanski et al. (2015) was run until 31-12-2005, and the modelled fluxes were for that reason evaluated for the overlapping period between model and flux tower observations from 07-08-2001 until 31-12-2005. For consistency, the new VOM runs were evaluated for the same time period.

To evaluate the foliage projected cover (FPC) dynamics of seasonal and perennial vegetation predicted by the VOM, we used satellite-derived monthly fractions of Photosynthetically Active Radiation absorbed by vegetation (fPAR) from Donohue et al. (2008, 2013), which were converted into estimates of FPC. The maximum possible value of fPAR was defined as 0.95 by Donohue et al. (2008) and relates to maximum projective cover (i.e. FPC = 1.0). The linear relation of FPC with fPAR-data (Asrar et al., 1984; Lu, 2003) allowed for the calculation of FPC by dividing the fPAR-values by the maximum value of 0.95.

2.2.8 Modifications to the VOM set-up

In comparison with previous applications of the VOM (Schymanski et al., 2009, 2015), several changes were made regarding the input data and process representation. Each individual change was added to the reference set-up of Schymanski et al. (2015) to assess the sensitivity of the model results for that change (see also Supplement S1). Briefly, the changes were assessed by the following cases:

---

[6]see also https://vom.readthedocs.io/en/latest/soildata.html

Table 2. Vertical profile of soil characteristics at Howard Springs, based on data from the Soil and Landscape Grid of Australia (Viscarra Rossel et al., 2014a,b,c), in addition to field measurements of J. Beringer and L. B. Hutley. Here, θ_r refers to the residual moisture content, θ_s the saturated water content, α and n the Van Genuchten soil parameters (Van Genuchten, 1980) and K_{sat} the saturated hydraulic conductivity.

Howard Springs	Soil type	θ_r (-)	θ_s (-)	α (1/m)	n (-)	K_{sat} (m/s)
0.00-0.20m	Sandy Loam	0.065	0.41	7.5	1.89	$1.228 * 10^{-5}$
0.20-0.40m	Sandy Loam	0.065	0.41	7.5	1.89	$1.228 * 10^{-5}$
0.40-0.60m	Sandy Clay Loam	0.1	0.39	5.9	1.48	$3.639 * 10^{-6}$
0.60-bedrock	Sandy Clay Loam	0.1	0.39	5.9	1.48	$3.639 * 10^{-6}$

- Reproduction the results of (Schymanski et al., 2015): the VOM was run with the same vegetation parameters and input data as (Schymanski et al., 2015), in order to check the new version of the VOM-code for reproducibility. The model was run from 1-1-1976 until 31-12-2005.

- Re-run SCE: the VOM was re-optimized with the same settings and input data as (Schymanski et al., 2015), in order to assess wheter the optimization algorithm converges to the same results as (Schymanski et al., 2015). The model was run from 1-1-1976 until 31-12-2005.

- Variable CO_2-levels: instead of using static atmospheric CO_2-concentrations of 350 ppm, the CO_2-concentrations from the Mauna Loa CO_2-records (Keeling et al., 2005) were used in the new model runs. The model was optimized here for the period 1-1-1976 until 31-12-2005.

- Reduced soil layer thickness: the soil layer thickness was set to 0.2 m, instead of the 0.5 m used by Schymanski et al. (2015), after running a sensitivity analyses (see also Supplement S2). The model was optimized here for the period 1-1-1976 until 31-12-2005.

- Variable atmospheric pressure: a new version of the meteorological data from the Australian SILO Data Drill (Jeffrey et al., 2001) provided time series of atmospheric pressure starting from 1-1-1980, whereas originally this had been fixed at a level of 1013 hPa. The model was optimized here for the period 1-1-1980 until 31-12-2005, due to the available time series from 1-1-1980.

- Optimized grass rooting depth: the rooting depth of grasses was prescribed at 1.0 m by Schymanski et al. (2009, 2015), which is roughly the position of a hard pan in the soil profile at Howard Springs. In this study, grass rooting depth is optimized along with the tree rooting depth at each site separately. The model was optimized here for the period 1-1-1976 until 31-12-2005.

– Updated meteorological data: a new version of the meteorological data from the Australian SILO Data Drill (Jeffrey et al., 2001) was used, starting from 1-1-1980. Therefore, the model was optimized here for the period 1-1-1980 until 31-12-2005. The time series of daily maximum and minimum temperatures, shortwave radiation, precipitation, vapour pressure and atmospheric pressure were all updated, but the CO_2-concentrations kept fixed at 350 ppm.

– Updated and extended meteorological data: the new version of the meteorological data from the Australian SILO Data Drill (Jeffrey et al., 2001) covers also more recent years. Therefore, the model period was extended and the model was optimized from 1-1-1980 until 31-12-2017. The time series of daily maximum and minimum temperatures, shortwave radiation, precipitation, vapour pressure and atmospheric pressure were all updated, but the CO_2-concentrations kept fixed at 350 ppm.

– Modified hydrology: in order to simulate freely draining conditions over the transect, in accordance with model simulations reported by Whitley et al. (2016), the position of drainage channels was set to 25 m below the surface and drainage parameters were set in a way to not let groundwater rise significantly above this (see also sect 2.2.5). The model was optimized here for the period 1-1-1976 until 31-12-2005.

– Modified soil properties: To improve realism, physical soil properties were not assumed to be vertically homogeneous, but varied with 20 cm depth increments (Table 2). Soil textures in the top 10 cm were based on field measurements provided by L. B. Hutley and J. Beringer, whereas the soil textures for the deeper soil layers were based on data from the Soil and Landscape Grid of Australia (Viscarra Rossel et al., 2014a,b,c). As a result, the soil profile at Howard Springs is now assumed to consist of sandy loam in the top 0.4 m and sandy clay loam below, whereas Schymanski et al. (2015) assumed the soil to be sandy loam in the entire soil profile. The model was optimized here for the period 1-1-1976 until 31-12-2005.

– Modified soil properties and hydrology: the modified soils and hydrology, as described above, will strongly interact. For that reason, their combined effect was assessed by implementing both changes in the set-up of Schymanski et al. (2015), keeping everything else constant.

3 Results

3.1 Effects of modifications to the VOM

To compare previous simulations using the VOM (Schymanski et al., 2015) with the new VOM set-up that includes the modifications as outlined in Sect. 2.2.8, each modification was applied to the previous setup in a stepwise manner to quantify the influence of each change in isolation. The resulting simulations were compared with those presented in Schymanski et al. (2015) for the site Howard Springs. In general, sensitivities varied between +20% and -25% in total GPP and ET, and are summarized in Figure 3. See also Supplement S1 for detailed time series.
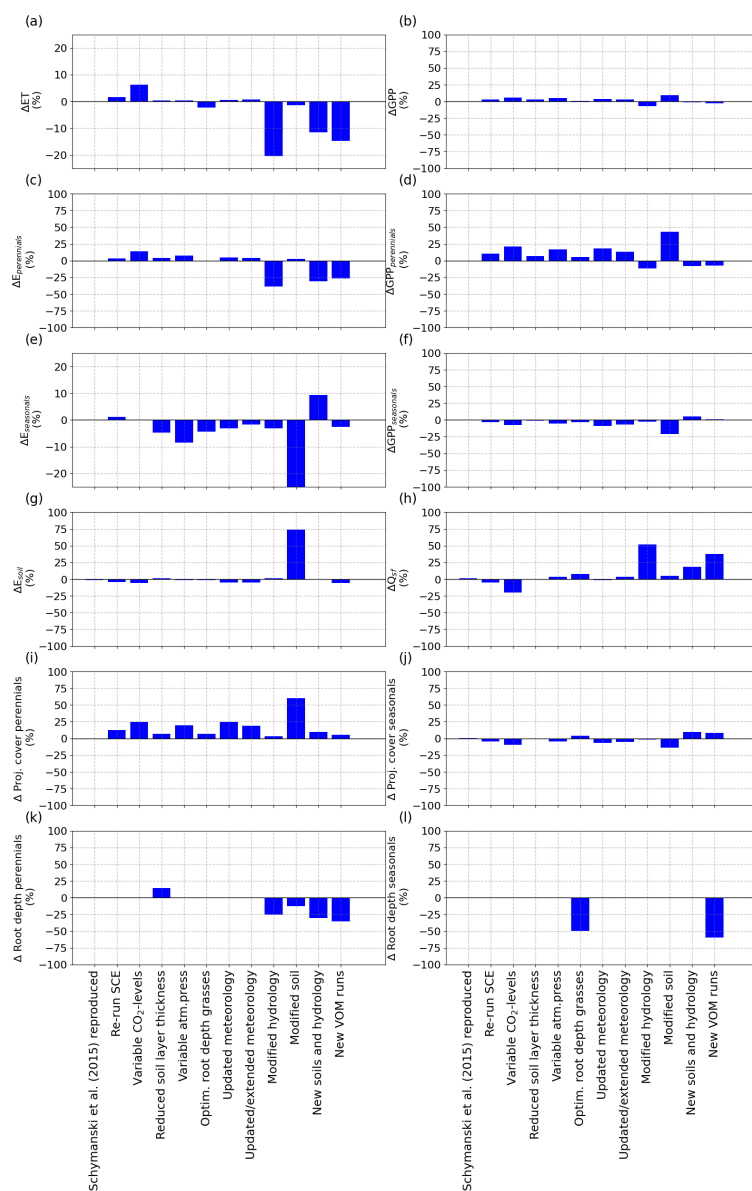
Figure 3. Relative changes in the annual values for the different (incremental) changes, as described in sect. 2.2.8, in comparison with Schymanski et al. (2015), with a) mean annual ET, b) mean annual GPP, c) transpiration perennials (trees), d) mean annual GPP perennials (trees), e) mean annual transpiration seasonals (grasses), f) mean annual GPP seasonals (grasses), g) mean annual soil evaporation, h) mean annual seepage face flow ($Q_s f$), i) prjected cover perennials (trees), j) projected cover seasonals (grasses), k) root depth perennials (trees) and l) root depth seasonals (grasses).
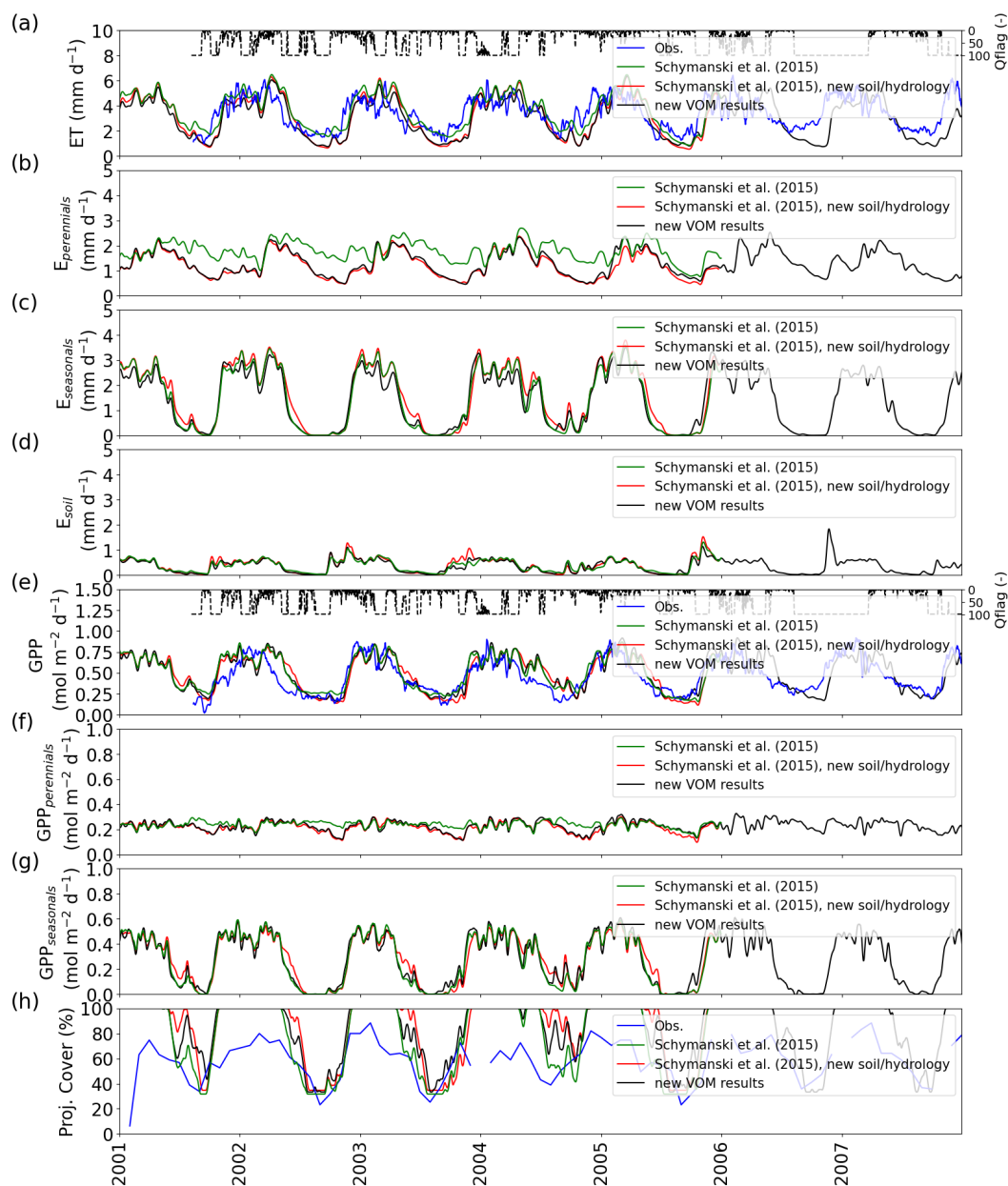
Figure 4. Comparison between the results of Schymanski et al. (2015) in green, simulations using new soil and hydrological parameterization (red), and simulations using all changes in combination (black). a) ET, b) transpiration by perennials (trees), c) transpiration seasonals (grasses), d) soil evaporation, e) GPP, f) GPP perennials (trees), g) GPP seasonals (grasses), and h) projective cover. Time series in a)-g) were smoothed using a moving average of 7 days. The daily average quality flags of the flux tower observations are shown as a dashed line in Panel (e), with a value of 100 for a completely gap-filled day and 1 for gap-free observations.

Table 3. Vegetation properties in the Vegetation Optimality Model optimized for maximizing the Net Carbon Profit.

Parameter	Description	Initial range	Timescale	Unit
$c_{\lambda f,p}$	water use parameter perennial vegetation	0.0 - 10000.0	Long-term	mol mol^{-1} m^{-1}
$c_{\lambda e,p}$	water use parameter perennial vegetation	-3.0 - 0.0	Long-term	-
$c_{\lambda f,s}$	water use parameter seasonal vegetation	0.0 - 10000.0	Long-term	mol mol^{-1} m^{-1}
$c_{\lambda e,s}$	water use parameter seasonal vegetation	-3.0 - 0.0	Long-term	-
$M_{A,p}$	fractional cover perennial vegetation	0 - 1	Long-term	-
$y_{r,p}$	rooting depth perennial vegetation	1.0 - 9.0	Long-term	m
$y_{r,s}$	rooting depth seasonal vegetation	0.05 - 2	Long-term	m
$M_{A,s}$	fractional cover seasonal vegetation	0.00 - (1.0-pct)	Daily	-
$J_{max25,p}$	electron transport capacity perennial vegetation	-	Daily	mol s^{-1} m^{-2}
$J_{max25,s}$	electron transport capacity annual vegetation	-	Daily	mol s^{-1} m^{-2}
$G_{s,p}$	stomatal conductance perennial vegetation	-	Daily	mol s^{-1} m^{-2}
$G_{s,s}$	stomatal conductance seasonal vegetation	-	Daily	mol s^{-1} m^{-2}
$S_{Adr,i,s}$	root surface area distribution of perennial vegetation	-	Daily	m^2 m^{-3}
$S_{Adr,i,s}$	root surface area distribution of annual vegetation	-	Daily	m^2 m^{-3}

The updated meteorological input data, for the runs until 31-12-2005 as well as the extended runs until 31-12-2017, hardly influenced the outcomes, with less than 10% relative change in the resulting fluxes (Figure 3a and b). However, a higher

260 contribution of the perennial vegetation in the fluxes can be observed, related to an increase in perennial vegetation cover (Figure 3i). This happened as well for re-running the SCE-algorithm, pointing at a relatively large uncertainty in the predicted perennial cover, with a range of values that results in similar fluxes.

Changing the fixed atmospheric CO$_2$-levels (350 ppm) in the set-up of Schymanski et al. (2015) to variable atmospheric CO$_2$-levels had a relatively large influence on perennial vegetation, yielding values of GPP for perennial vegetation that were

265 up to 21.0% higher (Figure 3d). Note that the CO$_2$-levels of the Mauna Loa records have a mean of 369 ppm and a maximum of 410 ppm during the modelling period, i.e. mostly higher than the 350 ppm prescribed in Schymanski et al. (2015), who also simulated an increase in GPP by perennial plants in response to elevated CO$_2$. See Figure S3.1f in Supplement S3 for more details about the CO$_2$-levels used here.

Changing the vertical soil discretization of 0.5 m in Schymanski et al. (2015) to a finer resolution of 0.2 m had a minor

270 influence, with a change of 2.6 % in the resulting GPP and 0.3 % in ET (Figure 3b, a). Similarly, when the grass rooting depths were optimized instead of the prescribed grass rooting depth of 1 m (everything else being the same as in Schymanski et al. (2015)), simulated GPP and ET were changed by 1.0% and -2.3% respectively (Figure 3b and a). The optimization led to shallower grass roots of 0.5 m (incurring lower carbon costs) and therefore to reductions in GPP and ET.

Stronger effects were found for the updated soil texture, which resulted in slightly reduced ET (-1.5%) but clearly increased

275 GPP by 9.5% (Figure 3a and b). The reduction in ET for an updated soil texture was mainly due to a large reduction in transpiration by seasonal vegetation. At the same time, simulated soil evaporation was increased, relating to an increased soil water storage and pointing at a reduced ability of the roots to take up water due to reduced hydraulic conductivity in the soil. The increase in simulated GPP was largely due to increased GPP by perennial vegetation, which at the same time slightly increased its transpiration. These changes were connected to a largely increased perennial vegetation cover and reduced rooting

280 depth compared to the original simulations (vegetation cover went up to 0.51 from 0.31, while rooting depth went down to 3.5 m from 4 m). Overall, the perennial vegetation benefited from the finer soil texture due to larger soil moisture storage capacity and carry-over of soil moisture into the dry season, whereas the seasonal vegetation suffered from reduced root water uptake due to lower hydraulic conductivity and increased soil evaporation during the wet season.

The implementation of free draining conditions had strong effects on the simulated fluxes as well, with lower values of

285 both ET and GPP (-20.4% and -6.9% respectively, Figure 3a and b). However, here especially the simulated ET of perennial vegetation was reduced, whereas the transpiration by seasonal vegetation stayed relatively similar (Figure 3c and e). This is because in the original simulations, capillary rise from the water table was most important during the dry season, when seasonal vegetation is inactive, and a change in the water table due to free draining conditions affects therefore mostly the perennial and not so much the seasonal vegetation.

290 Combining the new soils with the new hydrological settings still resulted in a reduction in ET by -11.5%, whereas their combined effect on GPP led to only a small reduction by -1.1% (Figure 3a and b). Here, the reduction of ET occured mainly during the wet season, and related to reductions in the perennial transpiration (Figure 4a-c), whereas the GPP stayed relatively similar (Figure 4e).

These findings are in accordance with the isolated effects of the new soils and hydrology, where free drainage conditions

295 resulted in a large reduction in ET and GPP, while finer soil texture resulted in a small reduction in ET but large increase in GPP. Hence, the finer soil texture largely compensated the effect on GPP, but not on ET.

The other changes had smaller effects on the fluxes, so we do not discuss them here individually. Instead, we will perform a more in-depth analysis of the differences in model results when all changes were combined.

3.2 Resulting differences

300 After incorporating all the changes, the relative error for mean annual evapo-transpiration (ET) changed from an overestimation by 8.4% to an underestimation of -10.2%, whereas the relative error for the mean annual GPP changed from 17.8% to 14.7%. The ensemble years in Figure 5 revealed that the evapo-transpiration (ET) was most strongly underestimated by the VOM during the dry season at Howard Springs. The observed groundwater tables (Figure 6a) ranged from 5-15 m depth seasonally, whereas the VOM was parameterized now to keep groundwater tables close to 25 m depth, for consistence with free drainage

305 conditions in other models. Schymanski et al. (2015) originally assumed a much shallower drainage level at Howard Springs, which led to groundwater tables around 5 meters depth, and better correspondence with the observed fluxes (Fig. 5).
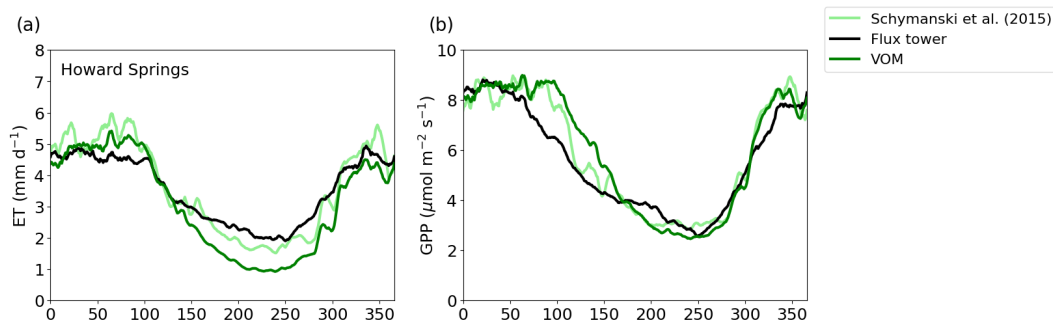
Figure 5. Ensemble years of evapo-transpiration (ET) and gross primary productivity (GPP) for the VOM (dark green), flux tower observations (black), results of Schymanski et al. (2015) (light green), all smoothed by a 7-day moving average. The ensemble years are calculated for the overlapping time periods with the flux tower observations (7-8-2001 until 21-12-2016).

The simulated soil moisture in the top soil layer, as illustrated in Fig. 6b, remained similar to the soil moisture values of Schymanski et al. (2015). The higher vertical resolution in the new model runs (20 cm cf. 50 cm soil layers) resulted in stronger surface soil moisture spikes around rainfall events, which makes the red line appear generally more noisy than the green line in Fig. 6b. Observed soil moisture in the upper 5 cm was generally lower than the simulated soil moisture in the top soil layer, particularly in the wet season. The total water storage in the top 5 m of the soil profile was substantially higher (up to 5-fold) in the new model simulations compared to Schymanski et al. (2015) (Figure 6c). The water retention curves (Figure 7) also show a clear shift, especially for the layers below 0.4 m, indicating extra storage. However, the water potentials again showed strong similarities between the current model runs and the results of Schymanski et al. (2015) (Figures 6d and e, respectively), with differences reflecting the vertical resolutions of the soil domains and simulated rooting depths.

4 Conclusions

The Vegetation Optimality Model has undergone several changes regarding model set-up and input data since its last application by Schymanski et al. (2015). The modifications consisted of updated and extended input data, the use of variable atmospheric CO_2-levels, modified soil properties, modified drainage levels as well as the addition of grass rooting depths to the optimized vegetation properties. The changes were applied to the VOM in a step-wise manner, by applying each modification to the previous set-up of Schymanski et al. (2015) in isolation to evaluate its effect on the results, before combining all modifications and analyzing their effect in combination. This analysis revealed that updated soil textures and a changed hydrological schematization had a strong influence on the results. An underestimation of dry season ET at Howard Springs was much more apparent when compared to the results of Schymanski et al. (2015), where the drainage parameterization maintained a water table depth much closer to the observed water table at this site. The effect of a much deeper groundwater table in the present simulations was partly buffered by a more fine-grained soil texture below 0.4 m (sandy clay loam instead of sandy loam), which resulted in an increase in water storage at otherwise similar water potentials in the top 5 m of soil compared to the simulations
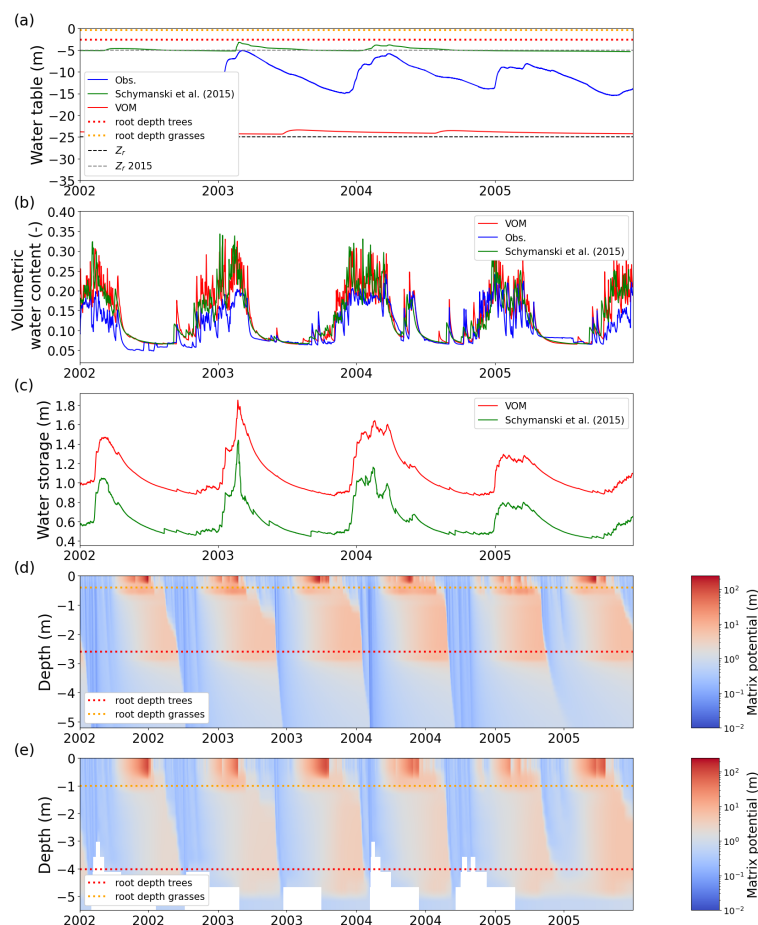
Figure 6. Simulated and observed hydrological state variables at Howard Springs. (a) groundwater depths, with dashed lines representing the prescribed bedrock depths, dotted lines the rooting depths (trees in red and grasses in orange), the VOM-results in red, the results of Schymanski et al. (2015) in green, and observations of three different bore holes in the vicinity of the study site in blue (Northern Territory Government, Australia, 2018); (b) the volumetric water content in the upper soil layer with the VOM results in red, the results of Schymanski et al. (2015) in green and measurement-based values at 5 cm depth at the flux tower sites in blue; (c) the total water storage in the upper 5 m for the VOM (red) and the results of Schymanski et al. (2015) in green; (d) the matrix water potentials for the current model runs of the VOM; and (e) the matrix water potentials of Schymanski et al. (2015). Observed water tables in Panel a) were obtained from the Water data portal, (Northern Territory Government, Australia, 2018, accessed 8-3-2019).

by Schymanski et al. (2015). The use of variable atmospheric CO_2-levels also had a strong influence on the results, which is especially important as the model time period has been extended in this study. This was mainly due to generally higher levels

330 of atmospheric CO_2 in recent observations, compared to the constant values used by Schymanski et al. (2015).

The stepwise analysis of modifications to a model setup and comparison against a benchmark dataset proved very helpful for identifying sensitivities of simulations to the different changes that might otherwise remain undiscovered due to compensating
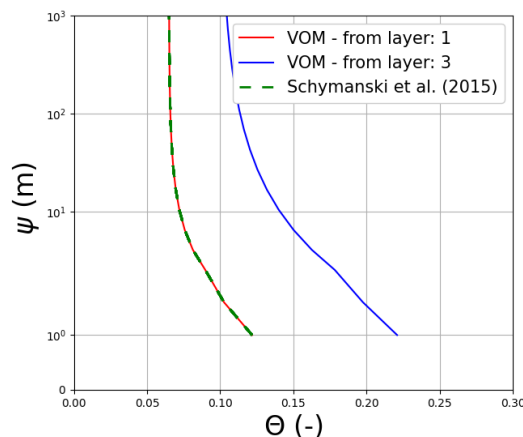
Figure 7. Water retention curves at Howard Springs for the current VOM-results (red: top two layers, blue: deeper layers), and the results of Schymanski et al. (2015) in green. Note that multiple red lines are shown due to the different soil parameterizations per soil layer in the current model runs, whereas Schymanski et al. (2015) used one soil parameterization for all soil layers. The upper soil layers have however the same soil parameters, leading to overlapping curves (red and dashed green).

effects of the various modifications during model development. In this way, we found that the neglect of a varying water table may have a strong effect on simulated surface fluxes, especially when soils are highly permeable. The common assumption of

335   free draining conditions in modelling studies should be revised, and if such an assumption is necessary, due to a lack of better hydrological understanding of a given site, or for comparison with other model simulations using this assumption (e.g. Whitley et al., 2016), potential bias in simulation results has to be acknowledged.

Code and data availability. Model code is available on github (https://github.com/schymans/VOM), release v0.5 is used in this study (http://doi.org/10.5281/zenodo.3630081). The full analysis including all scripts and data are available on renku (https://renkulab.io/gitlab/remko.

340   nijzink/vomcases). Before final publication, static versions of these repositories will be uploaded to zenodo.org and receive a separate DOI.

Author contributions. SJS and RN designed the set-up of the study. Model code was originally developed by SJS, but updated and modified by RN. RN did the pre-processing, modelling and post-processing. LH and JB provided site-specific knowledge and data. The main manuscript was prepared by RN, together with input from SJS. LH and JB provided corrections, suggestions and textual inputs for the main manuscript.

345   *Competing interests.* The authors declare no conflict of interest

Acknowledgements. This study is part of the WAVE-project funded by the Luxembourg National Research Fund (FNR) ATTRACT programme (A16/SR/11254288).

This work used eddy covariance data collected by the TERN-OzFlux facility (http://data.ozflux.org.au/portal/home). OzFlux would like to acknowledge the financial support of the Australian Federal Government via the National Collaborative Research Infrastructure Scheme
350   and the Education Investment Fund.

We acknowledge the SILO Data Drill hosted by the Queensland Department of Environment and Science for providing the meteorological data (https://www.longpaddock.qld.gov.au/silo/).

We acknowledge the Scripps CO2 program (https://scrippsco2.ucsd.edu/data/atmospheric_co2/primary_mlo_co2_record.html) for the Mauna Loa Observatory Records.

355   We also acknowledge CSIRO for the Soil and Landscape Grid of Australia (https://aclep.csiro.au/aclep/soilandlandscapegrid/index.html) and the Australian monthly fPAR derived from Advanced Very High Resolution Radiometer reflectances - version 5 (https://data.csiro.au/dap/landingpage?pid=csiro:6084).

We acknowledge the Northern Territory Water Data WebPortal for the groundwater data (https://water.nt.gov.au/).

References

360   Allen, R. G., Pereira, L. S., Raes, D., and Smith, M.: Crop evapotranspiration - Guidelines for computing crop water requirements, Irrigation and drainage paper 56, FAO - Food and Agriculture Organization of the United Nations, Rome, 1998.

Asrar, G., Fuchs, M., Kanemasu, E. T., and Hatfield, J. L.: Estimating Absorbed Photosynthetic Radiation and Leaf Area Index from Spectral Reflectance in Wheat1, Agronomy Journal, 76, 300, https://doi.org/10.2134/agronj1984.00021962007600020029x, https://www.agronomy.org/publications/aj/abstracts/76/2/AJ0760020300, 1984.

365   Beringer, J., Hutley, L. B., McHugh, I., Arndt, S. K., Campbell, D., Cleugh, H. A., Cleverly, J., Resco de Dios, V., Eamus, D., Evans, B., Ewenz, C., Grace, P., Griebel, A., Haverd, V., Hinko-Najera, N., Huete, A., Isaac, P., Kanniah, K., Leuning, R., Liddell, M. J., Macfarlane, C., Meyer, W., Moore, C., Pendall, E., Phillips, A., Phillips, R. L., Prober, S. M., Restrepo-Coupe, N., Rutledge, S., Schroder, I., Silberstein, R., Southall, P., Yee, M. S., Tapper, N. J., van Gorsel, E., Vote, C., Walker, J., and Wardlaw, T.: An introduction to the Australian and New Zealand flux tower network –OzFlux, Biogeosciences, 13, 5895–5916, https://doi.org/10.5194/bg-13-5895-2016,
370   https://www.biogeosciences.net/13/5895/2016/, 2016.

Beringer, J., McHugh, I., Hutley, L. B., Isaac, P., and Kljun, N.: Technical note: Dynamic INtegrated Gap-filling and partitioning for OzFlux (DINGO), Biogeosciences, 14, 1457–1460, https://doi.org/10.5194/bg-14-1457-2017, https://www.biogeosciences.net/14/1457/2017/, 2017.

Bierkens, M. F. P. and van den Hurk, B. J. J. M.: Groundwater convergence as a possible mechanism for multi-year persistence in rain-
375   fall, Geophysical Research Letters, 34, https://doi.org/10.1029/2006GL028396, http://agupubs.onlinelibrary.wiley.com/doi/abs/10.1029/2006GL028396, 2007.

Carsel, R. F. and Parrish, R. S.: Developing joint probability distributions of soil water retention characteristics, Water Resources Research, 24, 755–769, https://doi.org/10.1029/WR024i005p00755, http://agupubs.onlinelibrary.wiley.com/doi/abs/10.1029/WR024i005p00755, _eprint: https://onlinelibrary.wiley.com/doi/pdf/10.1029/WR024i005p00755, 1988.

380   Cowan, I. R. and Farquhar, G. D.: Stomatal Function in Relation to Leaf Metabolism and Environment, in: Integration of activity in the higher plant, edited by Jennings, D. H., pp. 471–505, Cambridge University Press, Cambridge, 1977.

Donohue, R., McVicar, T., and Roderick, M.: Australian monthly fPAR derived from Advanced Very High Resolution Radiometer reflectances - version 5. v1. CSIRO. Data Collection., https://doi.org/10.4225/08/50FE0CBE0DD06, 2013.

Donohue, R. J., Roderick, M. L., and McVicar, T. R.: Deriving consistent long-term vegetation information from AVHRR reflectance data
385   using a cover-triangle-based framework, Remote Sensing of Environment, 112, 2938–2949, https://doi.org/10.1016/j.rse.2008.02.008, http://linkinghub.elsevier.com/retrieve/pii/S0034425708000618, 2008.

Duan, Q., Sorooshian, S., and Gupta, V. K.: Optimal use of the SCE-UA global optimization method for calibrating watershed models, Journal of Hydrology, 158, 265–284, https://doi.org/10.1016/0022-1694(94)90057-4, http://www.sciencedirect.com/science/article/pii/0022169494900574, 1994.

390   Hutley, L. B.: Vegetation Above Ground Biomass, Litchfield Savanna SuperSite, Tower Plot, 2013, https://supersites.tern.org.au/knb/metacat/supersite.118.6/html, 2015.

Hutley, L. B., Beringer, J., Isaac, P. R., Hacker, J. M., and Cernusak, L. A.: A sub-continental scale living laboratory: Spatial patterns of savanna vegetation over a rainfall gradient in northern Australia, Agricultural and Forest Meteorology, 151, 1417–1428, https://doi.org/10.1016/j.agrformet.2011.03.002, http://www.sciencedirect.com/science/article/pii/S0168192311000839, 2011.

395   Jeffrey, S. J., Carter, J. O., Moodie, K. B., and Beswick, A. R.: Using spatial interpolation to construct a comprehensive archive of Australian climate data, Environmental Modelling & Software, 16, 309–330, https://doi.org/10.1016/S1364-8152(01)00008-1, https://linkinghub.elsevier.com/retrieve/pii/S1364815201000081, 2001.

Keeling, C. D., Piper, S. C., Bacastow, R. B., Wahlen, M., Whorf, T. P., Heimann, M., and Meijer, H. A.: Atmospheric CO2 and 13CO2 Exchange with the Terrestrial Biosphere and Oceans from 1978 to 2000: Observations and Carbon Cycle Implications, in: A History of

400   Atmospheric CO2 and its effects on Plants, Animals, and Ecosystems, pp. 83–113, Springer Verlag, New York, editors: Ehleringer, J.R., T. E. Cerling, M. D. Dearing, 2005.

Lu, H.: Decomposition of vegetation cover into woody and herbaceous components using AVHRR NDVI time series, Remote Sensing of Environment, 86, 1–18, https://doi.org/10.1016/S0034-4257(03)00054-3, https://linkinghub.elsevier.com/retrieve/pii/S0034425703000543, 2003.

405   Maxwell, R. M., Chow, F. K., and Kollet, S. J.: The groundwater–land-surface–atmosphere connection: Soil moisture effects on the atmospheric boundary layer in fully-coupled simulations, Advances in Water Resources, 30, 2447–2466, https://doi.org/10.1016/j.advwatres.2007.05.018, https://linkinghub.elsevier.com/retrieve/pii/S0309170807000954, 2007.

Northern Territory Government, Australia: Water data portal, https://nt.gov.au/environment/water/water-information-systems/water-data-portal, 2018.

410   Reggiani, P., Sivapalan, M., and Hassanizadeh, S. M.: Conservation equations governing hillslope responses: Exploring the physical basis of water balance, Water Resources Research, 36, 1845–1863, https://doi.org/10.1029/2000WR900066, http://doi.wiley.com/10.1029/2000WR900066, 2000.

Savenije, H. H. G.: The importance of interception and why we should delete the term evapotranspiration from our vocabulary, Hydrological Processes, 18, 1507–1511, https://doi.org/10.1002/hyp.5563, http://onlinelibrary.wiley.com/doi/abs/10.1002/hyp.5563, _eprint:

415   https://onlinelibrary.wiley.com/doi/pdf/10.1002/hyp.5563, 2004.

Schymanski, S. J., Roderick, M. L., Sivapalan, M., Hutley, L. B., and Beringer, J.: A test of the optimality approach to modelling canopy properties and CO2 uptake by natural vegetation, Plant, Cell & Environment, 30, 1586–1598, https://doi.org/10.1111/j.1365-3040.2007.01728.x, http://www.blackwell-synergy.com/doi/abs/10.1111/j.1365-3040.2007.01728.x, 2007.

Schymanski, S. J., Roderick, M. L., Sivapalan, M., Hutley, L. B., and Beringer, J.: A canopy-scale test of the optimal water use hypothesis,

420   Plant Cell & Environment, 31, 97–111, https://doi.org/10.1111/j.1365-3040.2007.01740.x, http://www.blackwell-synergy.com/doi/abs/10.1111/j.1365-3040.2007.01740.x, 2008a.

Schymanski, S. J., Sivapalan, M., Roderick, M. L., Beringer, J., and Hutley, L. B.: An optimality-based model of the coupled soil moisture and root dynamics, Hydrology and Earth System Sciences, 12, 913–932, https://doi.org/10.5194/hess-12-913-2008, http://www.hydrol-earth-syst-sci.net/12/913/2008/, 2008b.

425   Schymanski, S. J., Sivapalan, M., Roderick, M. L., Hutley, L. B., and Beringer, J.: An optimality-based model of the dynamic feedbacks between natural vegetation and the water balance, Water Resources Research, 45, https://doi.org/10.1029/2008WR006841, https://agupubs-onlinelibrary-wiley-com.proxy.bnl.lu/doi/full/10.1029/2008WR006841, 2009.

Schymanski, S. J., Roderick, M. L., and Sivapalan, M.: Using an optimality model to understand medium and long-term responses of vegetation water use to elevated atmospheric CO2 concentrations, AoB Plants, 7, plv060, https://doi.org/10.1093/aobpla/plv060, http:

430   //aobpla.oxfordjournals.org/content/7/plv060, 2015.

Van Genuchten, M. T.: A Closed-form Equation for Predicting the Hydraulic Conductivity of Unsaturated Soils, Soil Science Society of America Journal, 44, 892–898, https://doi.org/https://doi.org/10.2136/sssaj1980.03615995004400050002x, http://acsess.onlinelibrary.wiley.com/doi/abs/10.2136/sssaj1980.03615995004400050002x, 1980.

Viscarra Rossel, R., Chen, C., Grundy, M., Searle, R., Clifford, D., Odgers, N., Holmes, K., Griffin, T., Liddicoat, C., and Kidd, D.: Soil and Landscape Grid National Soil Attribute Maps - Sand (3" resolution) - Release 1, https://doi.org/10.4225/08/546F29646877E, https://data.csiro.au/collections/#collection/CIcsiro:10149v5, type: dataset, 2014a.

Viscarra Rossel, R., Chen, C., Grundy, M., Searle, R., Clifford, D., Odgers, N., Holmes, K., Griffin, T., Liddicoat, C., and Kidd, D.: Soil and Landscape Grid National Soil Attribute Maps - Silt (3" resolution) - Release 1, https://doi.org/10.4225/08/546F48D6A6D48, https://data.csiro.au/collections/#collection/CIcsiro:10688v5, type: dataset, 2014b.

Viscarra Rossel, R., Chen, C., Grundy, M., Searle, R., Clifford, D., Odgers, N., Holmes, K., Griffin, T., Liddicoat, C., and Kidd, D.: Soil and Landscape Grid National Soil Attribute Maps - Clay (3" resolution) - Release 1, https://doi.org/10.4225/08/546EEE35164BF, https://data.csiro.au/collections/#collection/CIcsiro:10168v5, type: dataset, 2014c.

von Caemmerer, S.: Biochemical Models of Leaf Photosynthesis, vol. 2 of *Techniques in Plant Sciences*, CSIRO Publishing, Collingwood, 2000.

Whitley, R., Beringer, J., Hutley, L. B., Abramowitz, G., De Kauwe, M. G., Duursma, R., Evans, B., Haverd, V., Li, L., Ryu, Y., Smith, B., Wang, Y.-P., Williams, M., and Yu, Q.: A model inter-comparison study to examine limiting factors in modelling Australian tropical savannas, Biogeosciences, 13, 3245–3265, https://doi.org/10.5194/bg-13-3245-2016, http://www.biogeosciences.net/13/3245/2016/, 2016.

York, J. P., Person, M., Gutowski, W. J., and Winter, T. C.: Putting aquifers into atmospheric simulation models: an example from the Mill Creek Watershed, northeastern Kansas, Advances in Water Resources, 25, 221–238, https://doi.org/10.1016/S0309-1708(01)00021-5, https://linkinghub.elsevier.com/retrieve/pii/S0309170801000215, 2002.